NACA

RESEARCH MEMORANDUM

STABILITY INVESTIGATION OF A BLUNT CONE AND A BLUNT

CYLINDER WITH A SQUARE BASE AT MACH NUMBERS

FROM 0.64 TO 2.14

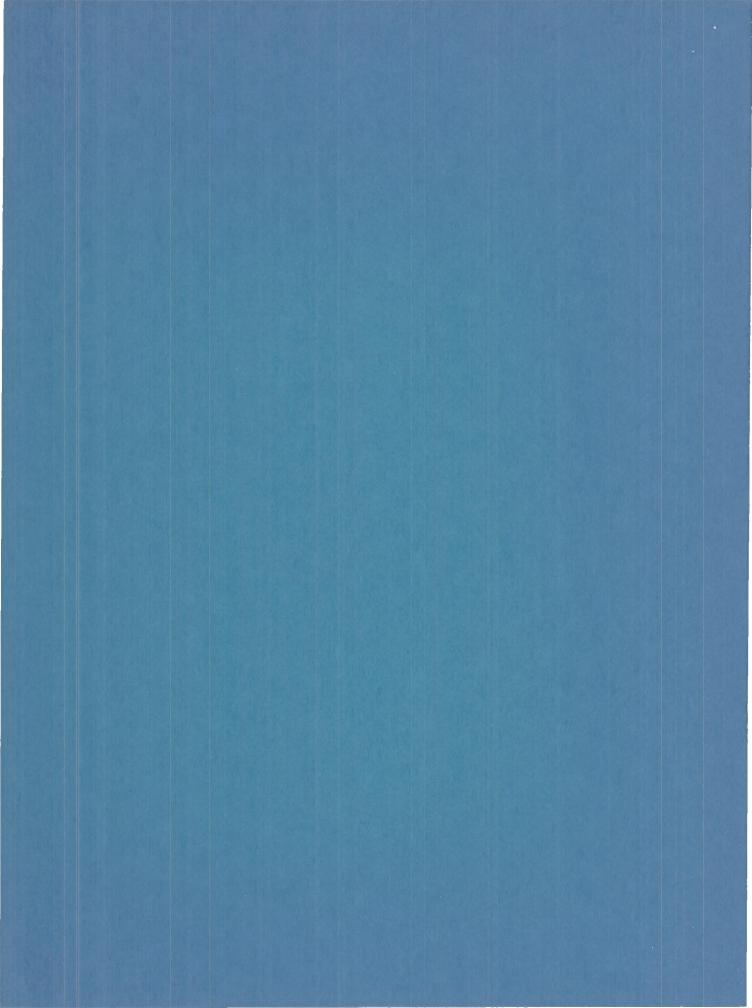By Lucille C. Coltrane

Langley Aeronautical Laboratory
Langley Field, Va.

Declassified March 12, 1964

NATIONAL ADVISORY COMMITTEE
FOR AERONAUTICS
WASHINGTON
September 17, 1958

NATIONAL ADVISORY COMMITTEE FOR AERONAUTICS

RESEARCH MEMORANDUM

STABILITY INVESTIGATION OF A BLUNT CONE AND A BLUNT

CYLINDER WITH A SQUARE BASE AT MACH NUMBERS

FROM 0.64 TO 2.14*

By Lucille C. Coltrane

SUMMARY

A fineness-ratio-2.6 bluff shape with an $x^{1/10}$ nose and a $5°$ flare extending the entire body length and a fineness-ratio-2.5 bluff shape with an $x^{1/10}$ nose and a square base with sides equal to the diameter of the cylindrical forebody have been tested in free flight over a Mach number range of 0.64 to 2.14 and a Reynolds number range of 1×10^6 to 10×10^6. Time histories, cross plots of force and moment coefficients, and plots of the longitudinal-force coefficient, rolling velocity, aerodynamic center, normal-force-curve slope, and dynamic stability are presented. With the center-of-gravity location at about 31 percent of the model length, the models were both statically and dynamically stable throughout the Mach number range with one exception. In the transonic range, the flared model was statically unstable and there may have been a region of dynamic instability in this range also. The average aerodynamic center of both models moved slightly rearward with increasing speed, and for each model the normal-force-curve slope was fairly constant throughout the supersonic speed range. The drag level of the two models is about 0.5 at subsonic speeds and 1.0 at supersonic speeds.

INTRODUCTION

An investigation is being conducted by the Langley Pilotless Aircraft Research Division to determine the dynamic-stability characteristics of bluff body shapes by means of the rocket-boosted free-flight-model technique. The results from flight tests of other bluff shapes in this program have been reported in references 1 and 2. This paper presents results from tests of a fineness-ratio-2.6 bluff shape with a $5°$ flare

---

*Title, Unclassified.

extending the entire body length and of a fineness-ratio-2.5 bluff shape having a square base with sides equal to the diameter of the cylindrical body. The nose shape of both models is defined by a curve of $x^{1/10}$. These tests covered a Mach number range from 0.64 to 2.14 and a Reynolds number range from 1×10^6 to 10×10^6 based on the reference diameter of 8 inches. The free-flight tests were conducted at the Langley Pilotless Aircraft Research Station at Wallops Island, Va.

SYMBOLS

The data are presented relative to the body-axis system and the positive directions of the force coefficients, moment coefficients, and angular velocities are shown in figure 1. The various symbols used throughout the paper are defined as follows:

a accelerometer reading, g units

C_C longitudinal-force coefficient, $a_{l,cg} \dfrac{W/S}{q}$

C_m pitching-moment coefficient, $\dfrac{I_Y}{qSd}(\ddot{\theta} - \dot{\psi}\dot{\phi})$

$C_{m_q} = \dfrac{dC_m}{d\dfrac{\dot{\theta}d}{2V}}$

C_N normal-force coefficient, $a_{n,cg} \dfrac{W/S}{q}$

$C_{N_\alpha} = \dfrac{dC_N}{d\alpha}$

C_n yawing-moment coefficient, $\dfrac{I_Z}{qSd}(\ddot{\psi} + \dot{\theta}\dot{\phi})$

C_Y lateral-force coefficient, $a_{t,cg} \dfrac{W/S}{q}$

d reference diameter, ft (fig. 2)

g acceleration due to gravity, ft/sec^2

I moment of inertia, $slug\text{-}ft^2$

I_X, I_Y, I_Z moments of inertia about X-, Y-, and Z-axis, slug-ft^2

k   radius of gyration, $\sqrt{\dfrac{I_Y}{m}}$, ft

l length of model, ft

M   Mach number

m   mass, slugs

q   dynamic pressure, lb/sq ft

R   Reynolds number based on reference diameter

S   cross-sectional area of model, sq ft

t   time, sec

V   free-stream velocity, ft/sec

W   weight of model, lb

x   distance along model from nose, ft; when used for accelerometer location, distance measured from center of gravity, positive forward, ft

y   distance from center line of model

α angle of attack, radians

θ angle of pitch, radians

λ_0 nonrolling damping constant, 1/sec

$\Delta\lambda$ damping constant due to roll, 1/sec

μ relative-density factor, $4m/\rho Sd$

ρ air density, slugs/cu ft

φ angle of roll, radians

ψ angle of yaw, radians

ω_0 basic oscillation frequency, radians/sec

$\Delta\omega$ component of total pitch frequency resulting directly from roll, radians/sec

$\ddot{\theta} - \dot{\psi}\dot{\phi}$ effective pitching acceleration, $g \dfrac{a_{n,2} - a_{n,1}}{x_{n,2} - x_{n,1}}$, radians/sec^2

$a_{n,cg}$ normal acceleration, $\dfrac{a_{n,1}x_{n,2} - a_{n,2}x_{n,1}}{x_{n,2} - x_{n,1}}$, g units

$\ddot{\psi} + \dot{\theta}\dot{\phi}$ effective yawing acceleration, $g \dfrac{a_{t,2} - a_{t,1}}{x_{t,2} - x_{t,1}}$, radians/sec^2

$a_{t,cg}$ transverse acceleration, $\dfrac{a_{t,1}x_{t,2} - a_{t,2}x_{t,1}}{x_{t,2} - x_{t,1}}$, g units

Subscripts:

ac   aerodynamic center

cg   center of gravity

l longitudinal

n   normal

t   transverse

1   forward end of model

2   rear end of model

A dot above a symbol indicates time rate of change of symbol, for example, $\dot{\theta} = \partial\theta/\partial t$.

MODELS

The physical characteristics of the models are presented in table I, and drawings of the models are shown in figure 2. Photographs of the models and model booster arrangements are presented in figure 3.

The flared model (designated model I), of fineness ratio 2.6, had a 5° flare extending the entire body length, and the model with a square

base (designated model II), of fineness ratio 2.5, had a circular cylinder forebody and a square afterbody with sharp corners. The center of gravity for model I was at 30.9 percent and for model II was at 30.7 percent of the model length. Each model had a nose shape defined by the equation $y = Cx^{0.1}$, where C is a numerical constant. The nose ordinates are given in table II. Each model contained two small pulse rockets which were mounted normal to the longitudinal axis and ahead of the center of gravity to give a yaw disturbance.

The models were constructed of steel and covered with a fiber-glass—plastic shell. The nose sections were machined from solid steel. The square-base afterbody of model II was constructed of laminated wood.

INSTRUMENTATION

Model instrumentation consisted of an NACA six-channel telemeter which transmitted data from six accelerometers located as follows: one normal and one transverse accelerometer in the forward end of the model, one normal and one transverse accelerometer in the rear of the model, and two longitudinal accelerometers, one for high range and one for low range, behind the center of gravity. A measure of the signal strength transmitted from the loop antenna provided an indication of the roll rate of the models since the strength of the signal varied with the model roll position.

Ground instrumentation included a CW Doppler radar unit to measure the velocity of the model, a modified SCR 584 tracking radar set to determine the flight path, and a rollsonde receiver used as an additional measure of the rolling velocity. Fixed and tracking motion-picture cameras were used to observe the model during the first portion of the flight. Atmospheric data were obtained from a rawinsonde released immediately before model flight.

TESTS AND ANALYSIS

The models were ground launched at an angle of 70° from the horizontal by means of a mobile launcher, as shown in figure 3(c). A solid-propellant Cajun rocket motor boosted the models to maximum velocity. Drag flaps were incorporated into the booster to increase the separating force between the model and booster at booster burnout. Tracking radar showed that the models followed an approximately parabolic flight path.

Data obtained from normal and transverse accelerometers located at two positions in the model were used to determine the pitching-moment and yawing-moment coefficients.

For the aerodynamic-center location, where

$$\frac{x_{ac}}{l} = -\frac{dC_m}{dC_N}\frac{d}{l} + \frac{x_{cg}}{l}$$

or

$$\frac{x_{ac}}{l} = -\frac{dC_n}{dC_Y}\frac{d}{l} + \frac{x_{cg}}{l}$$

(1)

the values for $\dfrac{dC_m}{dC_N}$ and $\dfrac{dC_n}{dC_Y}$ were taken directly from the polars of C_m against C_N and C_n against C_Y over the region found to be the most nearly linear.

The normal-force-coefficient curve slope per radian was determined by use of the following equation:

$$C_{N_\alpha} = \frac{-2\mu\left(\dfrac{d}{2V}\right)^2\left(\dfrac{k}{d}\right)^2}{\dfrac{dC_m}{dC_N}}\left[\omega_0{}^2 + \lambda_0{}^2 - \Delta\lambda^2 + \Delta\omega^2\,\frac{\dfrac{I_X}{I}\left(1 - \dfrac{I_X}{4I}\right)}{\left(1 - \dfrac{I_X}{2I}\right)^2}\right]$$

(2)

An indication of the dynamic stability was obtained from

$$C_{m_q} = 2\left(\frac{k}{d}\right)^2\left(\frac{2\mu d}{2V}\lambda_0 + C_{N_\alpha}\right)$$

(3)

This method of analysis for C_{N_α} and C_{m_q} is presented in more detail in references 2 and 3. Table III presents values of some of the terms used in the above equations.

ACCURACY

The possible systematic errors (zero shifts) due to instrument inaccuracies, estimated to be ±2 percent of the calibrated range of the instruments, are stated below in coefficient form for representative Mach numbers. The magnitude of the random errors is much smaller and

may be judged by the scatter of test points on the data figures.

Coefficient	Flared model (model I) at Mach number of -			Square-base model (model II) at Mach number of -		
	2.14	1.04	0.74	1.85	1.11	0.77
C_N	±0.038	±0.196	±0.416	±0.046	±0.147	±0.345
C_Y	±.037	±.190	±.404	±.048	±.152	±.359
C_C	±.040	±.044	±.092	±.053	±.035	±.083

PRESENTATION OF RESULTS

The variation of test Reynolds number, based on reference diameter, with test Mach number is presented in figure 4. The model flight paths are presented as the variation of altitude with horizontal distance in figure 5, and the variation of velocity and dynamic pressure with time is shown in figure 6.

Time histories of the normal-force coefficient, lateral-force coefficient, and Mach number are presented in figures 7 and 8 for model I and model II, respectively. Basic-data crossplots of force and moment coefficients are shown in figures 9 and 10. The rolling velocity is shown in figure 11 as a function of Mach number. The variation with Mach number of the average aerodynamic center, the normal-force-curve slope, the dynamic stability, and the measured longitudinal-force coefficient are presented in figures 12 to 15.

DISCUSSION OF RESULTS

Time History

The time histories of M, C_Y, and C_N for model I (fig. 7) and for model II (fig. 8) show the motion of the models caused by the separation from the booster rocket motor and by the firing of two pulse rockets. Throughout the flight a coupled motion with respect to the body-axis system was experienced by the models. Also, the appearance of a definite trim change can be observed. When given a disturbance at separation, the response of both models was a low-amplitude oscillation which

damped to a very low-amplitude oscillation that persisted throughout the supersonic speeds until the models were disturbed by the firing of a pulse rocket. The response here, in the transonic range, was a large-amplitude irregular oscillation with poor damping. When disturbed again by the firing of a second pulse rocket in the subsonic speed range, the response was an average-amplitude oscillation which damped to a low-amplitude sustained oscillation.

Basic-Data Plots

Cross plots of C_N and C_Y presented in figures 9 and 10 for various Mach numbers indicate the model motion. These plots are used in determining the values tabulated in table III by utilizing the method described in reference 3. From visual observation of these cross plots and comparison with similar plots of reference 3, it can be seen that the models remained below roll resonance. The angular displacement of adjacent peaks on the cross plot gives an indication of the rolling rate of the models, and the values obtained are shown in figure 11 with measured averages from the rollsonde.

Pitching- and yawing-moment coefficients as a function of force coefficients are shown in figures 9 and 10 for various Mach numbers. These variations show a stable slope which is quite linear in the supersonic speed range but somewhat nonlinear in the transonic and subsonic ranges. It is seen in figure 9(c) that the flared model was statically unstable near zero lift in the transonic speed range. Instrument inaccuracies probably account for the consistent drifting of the coefficients away from the zero axis.

Aerodynamic Center

The variation of the aerodynamic center with Mach number is shown in figure 12. The average aerodynamic center moved slightly rearward with increasing speeds. The models were statically stable throughout the Mach number range except for a limited region of instability experienced by the flared model. This fact was brought out in the preceding section.

Lift and Drag

The variation of the normal-force-curve slope with Mach number is shown in figure 13. The test points show that this variation was fairly constant throughout the speed range for both models, with model II experiencing a slightly higher C_{N_α} in the supersonic region.

The variation of longitudinal-force coefficient with Mach number is presented in figure 14. It is seen that the drag level of both models is about 0.5 at subsonic speed and 1.0 at supersonic speed. Model I has a slightly higher trend than model II throughout the test range but the difference is within the accuracy of the data.

Dynamic Stability

The dynamic stability of the models of this test, together with data from references 2 and 4, is shown in figure 15 as a function of Mach number. The models of this test were dynamically stable throughout the speed range. At transonic speeds there may have been a region of dynamic instability, but the data were not conclusive because of the irregular nature of the oscillations and the change in trim force coefficient.

The models of references 2 and 4 are seen to be dynamically stable in the supersonic and transonic regions but unstable dynamically in the subsonic region.

SUMMARY OF RESULTS

From flight tests, over a Mach number range of 0.64 to 2.14 and a Reynolds number range of 1×10^6 to 10×10^6, of a fineness-ratio-2.6 bluff shape with a 5^0 flare extending the entire body length and a fineness-ratio-2.5 bluff shape having a square base with sides equal to the diameter of the cylinder forebody, each with an $x^{1/10}$ nose shape, the following results were obtained. The models were both statically and dynamically stable throughout the Mach number range with one exception. In the transonic range, the flared model was statically unstable and there may have been a region of dynamic instability in this range also. The average aerodynamic center of both models moved slightly rearward with increasing speeds, and for each model the normal-force-curve slope was fairly constant throughout the speed range. The difference in the drag level of the two models was small. For both models the drag is about 0.5 at subsonic speed and 1.0 at supersonic speed.

Langley Aeronautical Laboratory,
      National Advisory Committee for Aeronautics,
            Langley Field, Va., July 10, 1958.

REFERENCES

1. McFall, John C., Jr.: Dynamic Stability Investigation of Two Right
   Circular Cylinders in Axial Free Flight at Mach Numbers From 0.4
   to 1.7 - Fineness-Ratio-2.56 Cylinder and Fineness-Ratio-4.0
   Cylinder With Flared Afterbody. NACA RM L56L28, 1957.

2. Coltrane, Lucille C.: Investigation of Two Bluff Shapes in Axial
   Free Flight Over a Mach Number Range From 0.35 to 2.15. NACA
   RM L58A16, 1958.

3. Nelson, Robert L.: The Motions of Rolling Symmetrical Missiles
   Referred to a Body-Axis System. NACA TN 3737, 1956.

4. Tom, William S.: Aerodynamic Characteristics of the ML-404-20
   Polaris Re-Entry Models; Preliminary Results. Tech. Note 5034-32,
   U. S. Naval Ord. Test Station (China Lake, Calif.), Nov. 14, 1957.

TABLE I.- PHYSICAL CONSTANTS FOR MODELS TESTED

Constant	Model I	Model II
W, lb	96.5	94.0
I_X, slug-ft^2 . .	0.166	0.138
I_Y, slug-ft^2 . .	0.770	0.686
I_Z, slug-ft^2 . .	0.770	0.686
$\dfrac{x_{cg}}{l}$	0.309	0.307
d, ft	0.667	0.667
l, ft	1.725	1.667
S, sq ft	0.348	0.348

TABLE II.- NOSE ORDINATES

$$\left[y = Cx^{0.1}; \text{ value of } y \text{ at } x = 0 \right.$$
$$\left. \text{arbitrarily set at } 1.600 \text{ in.} \right]$$

x, in.	y, in.
0	1.600
.01	2.198
.10	2.765
.20	2.964
.30	3.086
.40	3.177
.50	3.249
.60	3.309
.80	3.406
1.00	3.483
1.50	3.627
2.00	3.733
2.50	3.817
3.00	3.887
3.50	3.947
4.00	4.000

TABLE III.- VALUES USED TO DETERMINE SLOPE OF NORMAL-FORCE

COEFFICIENTS AND DYNAMIC STABILITY

Mach number	ω_0	λ_0	$\Delta\lambda$	$\Delta\omega$	$\dfrac{\dfrac{I_X}{I}\left(1 - \dfrac{I_X}{4I}\right)}{\left(1 - \dfrac{I_X}{2I}\right)^2}$	$\dfrac{dC_m}{dC_N}$ or $\dfrac{dC_n}{dC_Y}$
Model I						
2.14	51.0	-1.59	0	9.4	0.256	-0.375
1.94	43.0	-1.59	0	9.4	.256	-.360
[a]1.10	13.0	(b)	(b)	8.7	.256	.060
1.04	14.0	(b)	(b)	8.7	.256	(b)
.91	15.0	-.44	0	8.7	.256	-.210
.82	9.0	-.44	(c)	8.9	.256	-.125
.74	8.0	-.34	(c)	9.5	.256	-.135
.69	8.0	-.34	(c)	9.8	.256	-.135
.64	8.0	-.34	(b)	10.0	.256	(b)
Model II						
1.85	51.0	-1.08	0	1.8	0.236	-0.400
1.68	44.0	-1.08	0	.5	.236	-.370
1.50	36.0	-1.08	0	-.9	.236	-.330
1.11	17.0	-2.10	4.25	-2.9	.236	-.145
.98	13.0	(b)	(b)	-3.6	.236	-.110
.89	11.0	-.44	-2.09	-3.6	.236	-.135
.77	13.0	-.59	0	-3.3	.236	-.180
.71	10.0	-.59	(c)	-2.9	.236	-.180
.65	10.0	-.59	(c)	-2.8	.236	-.235

[a]Value obtained from only a portion of figure 9(c).

[b]Reliable value was not obtained.

[c]Reliable value was not obtained but assumed to be zero for calculations.
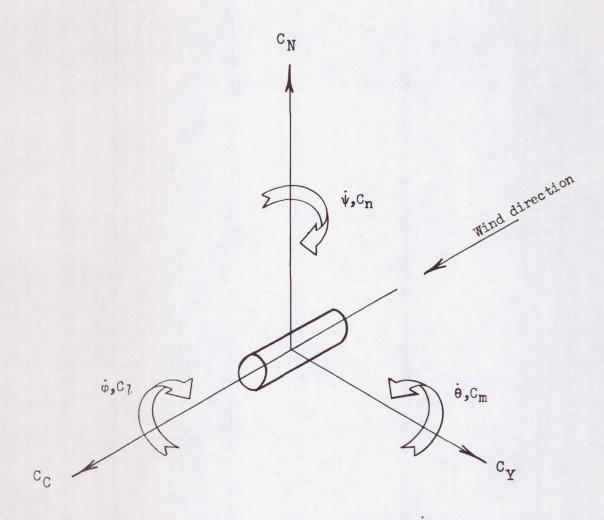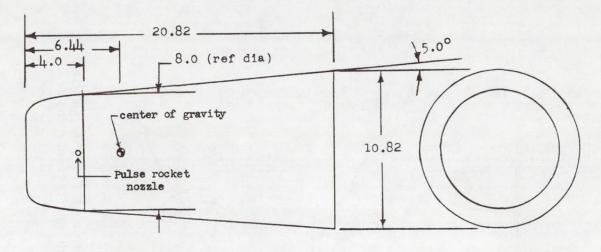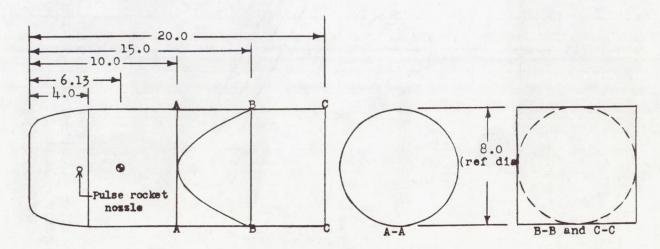
Figure 1.- Axis system with origin at center of gravity, showing
positive directions of force and moment coefficients and
angular velocities.
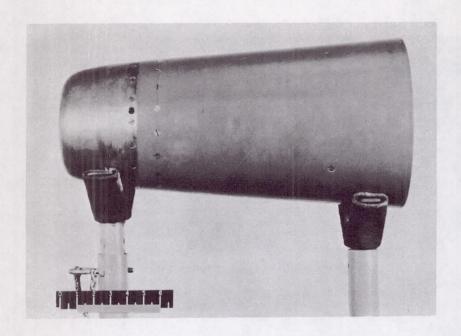
(a) Model I; fineness ratio of 2.60.
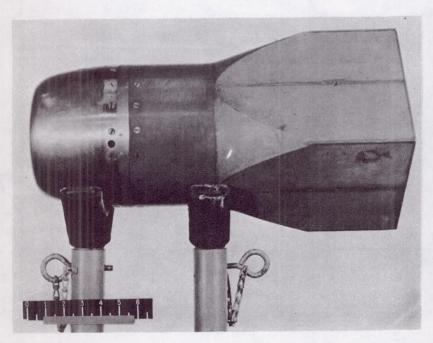
(b) Model II; fineness ratio of 2.50.

Figure 2.- Drawings of models tested. All dimensions are in inches.
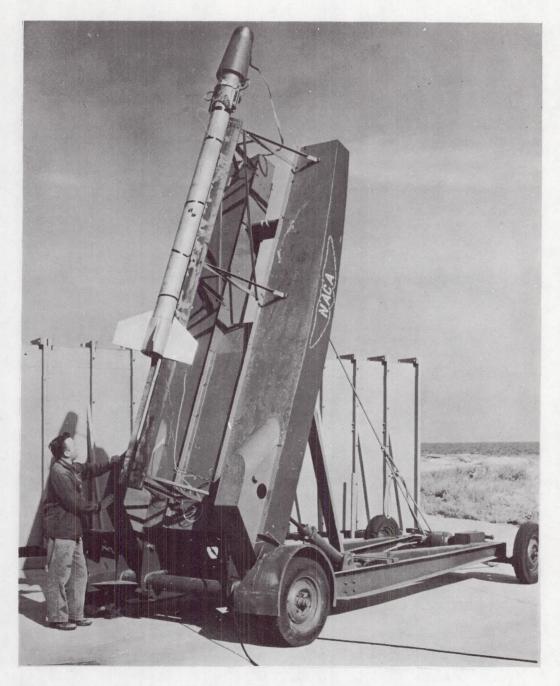
(a) Model I.

(b) Model II.   L-58-2512

Figure 3.- Photographs of models tested.

(c) Model I on booster in launching position.   L-57-4620.1

Figure 3.- Concluded.
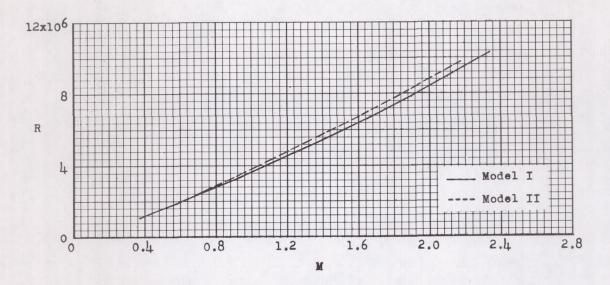
Figure 4.- Reynolds number of tests based on reference diameter.
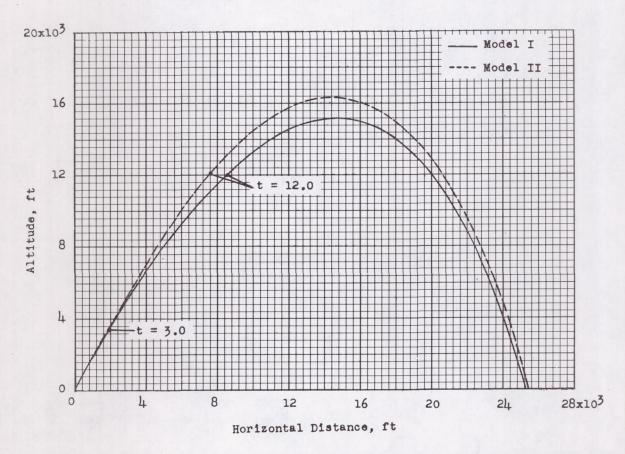
Figure 5.- Flight paths of models tested.
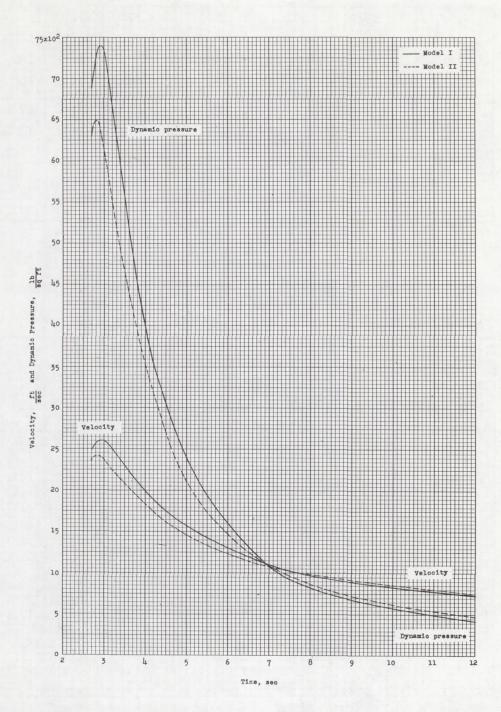
Figure 6.- Velocity and dynamic pressure of models tested.
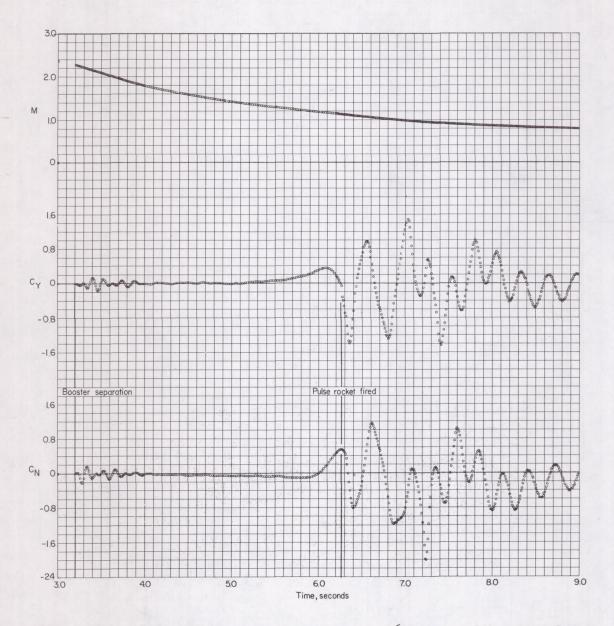
Figure 7.- Time history of fineness-ratio-2.60 shape with a rounded
nose and a 5° flared body. (Model I.)
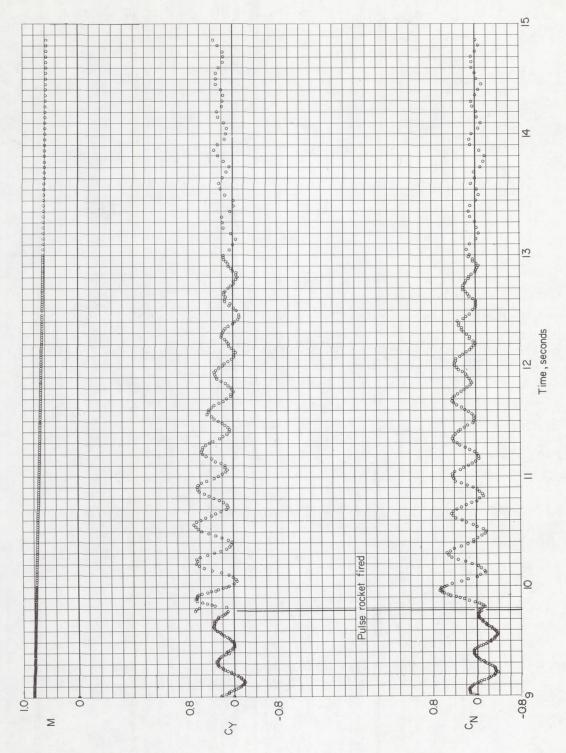
Figure 7.- Concluded.
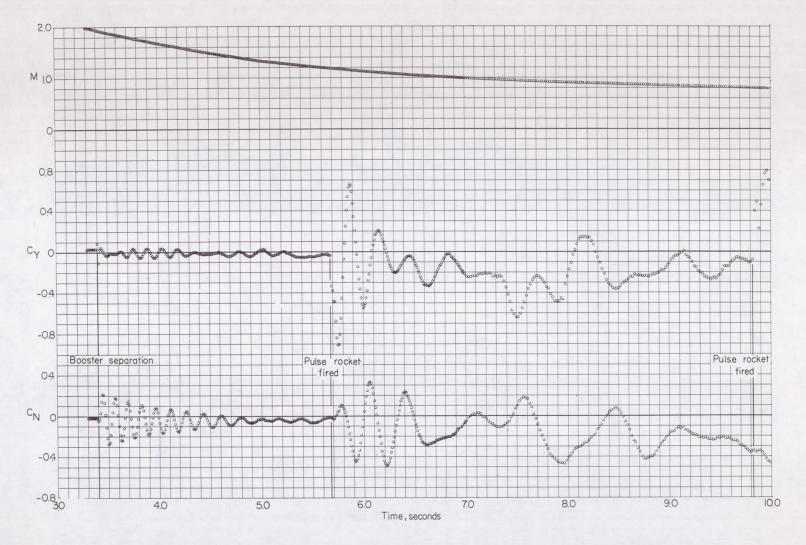
Figure 8.- Time history of fineness-ratio-2.50 shape with a rounded nose and a square afterbody (model II).
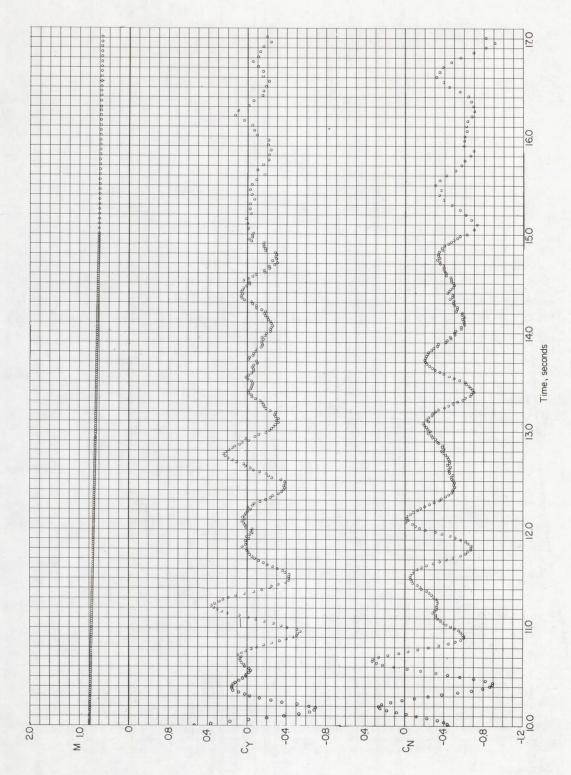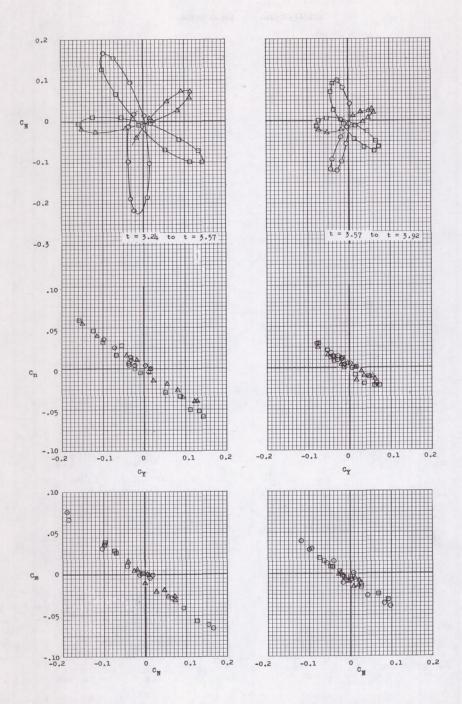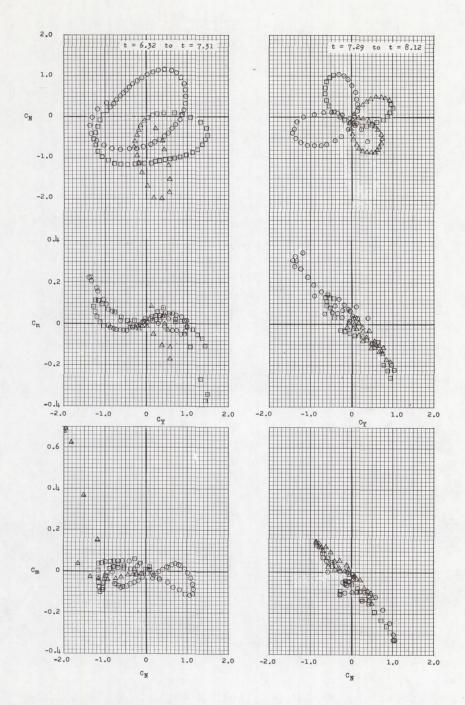
Figure 8.- Concluded.
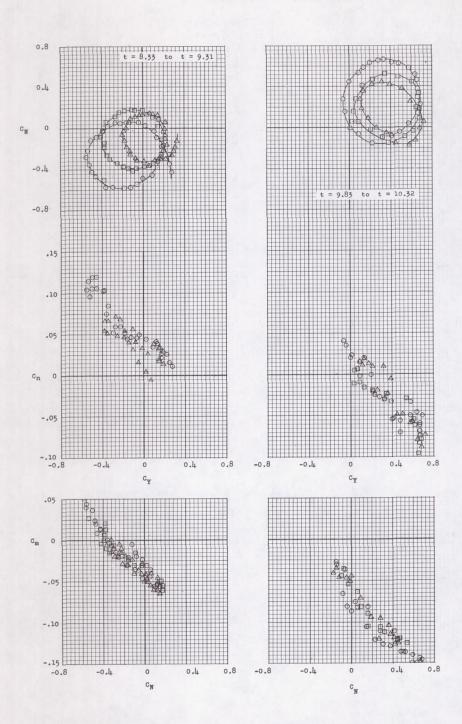
(a) M = 2.24 to M = 2.04. (b) M = 2.04 to M = 1.83.
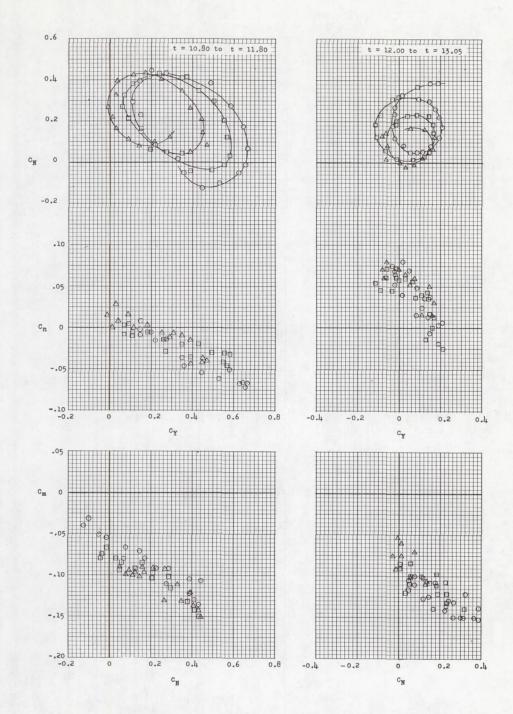
Figure 9.- Basic-data cross plots of force and moment coefficients.
  Model I. The time sequence is indicated by the symbols O,
  □, and △.

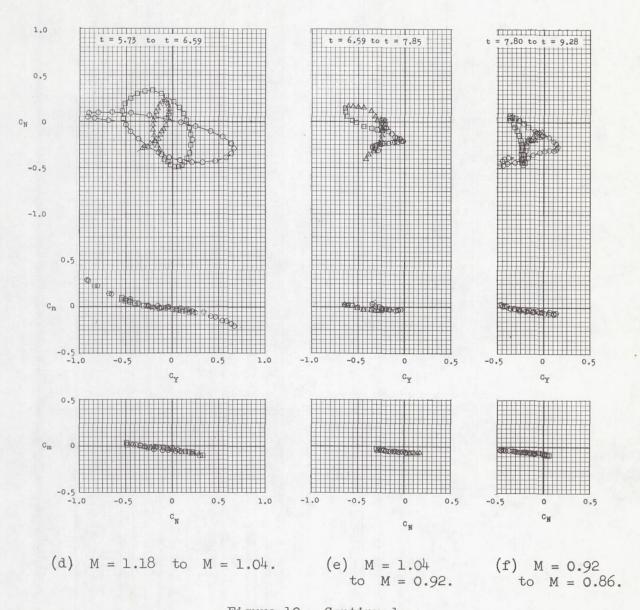(c) M = 1.12 to M = 0.95. (d) M = 0.95 to M = 0.87.

Figure 9.- Continued.

(e) M = 0.86 to M = 0.79. (f) M = 0.77 to M = 0.71.

Figure 9.- Continued.

(g) M = 0.71 to M = 0.67. (h) M = 0.66 to M = 0.62.

Figure 9.- Concluded.

(a) M = 1.93 to M = 1.77.   (b) M = 1.76   (c) M = 1.59
                                    to M = 1.59.   to M = 1.42.
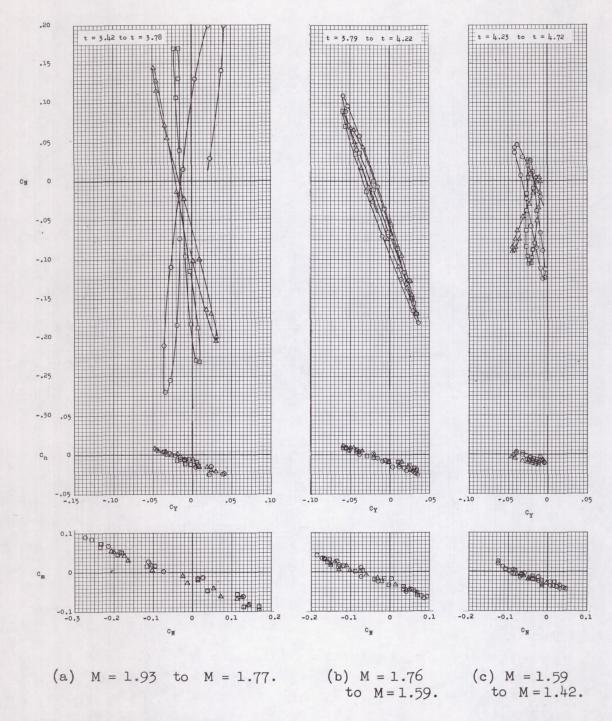
Figure 10.- Basic-data cross plots of force and moment coefficients.
   Model II. The time sequence is indicated by the symbols $\bigcirc$, $\square$,
   and $\triangle$.

(d) M = 1.18 to M = 1.04.   (e) M = 1.04   (f) M = 0.92
                                      to M = 0.92.   to M = 0.86.

Figure 10.- Continued.

(g) M = 0.80
to M = 0.74.

(h) M = 0.74
to M = 0.68.

(i) M = 0.68
to M = 0.62.
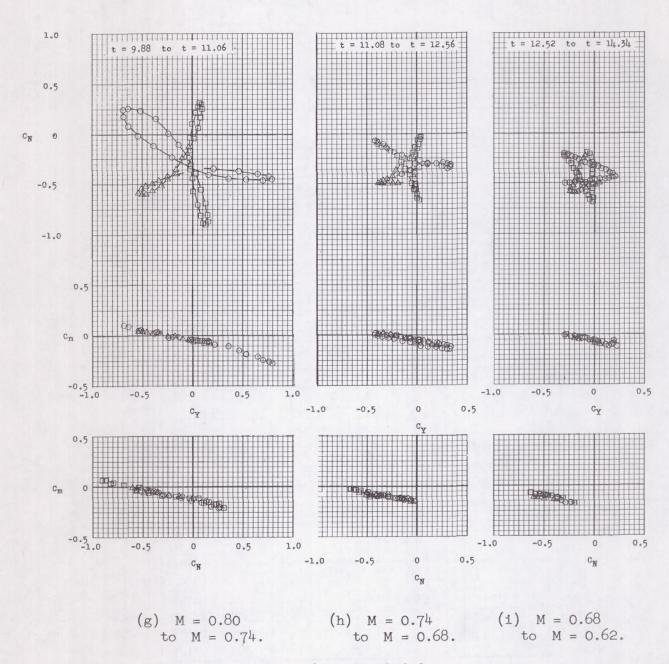
Figure 10.- Concluded.
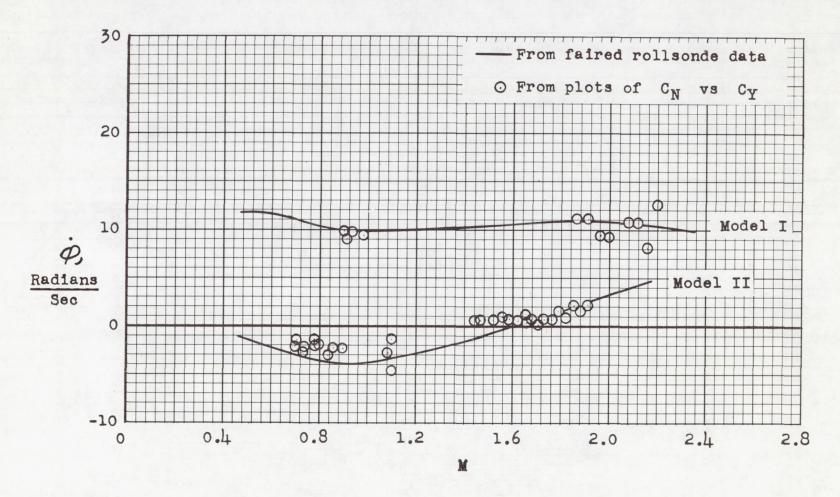
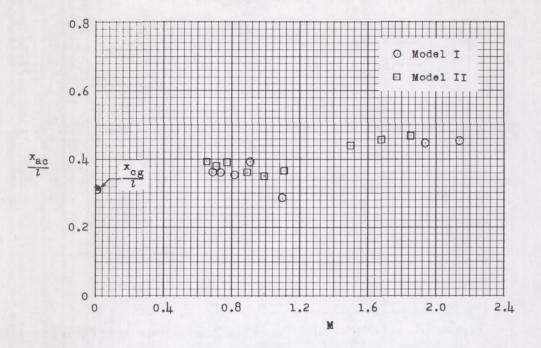Figure 11.- Variation of rolling velocity with Mach number.

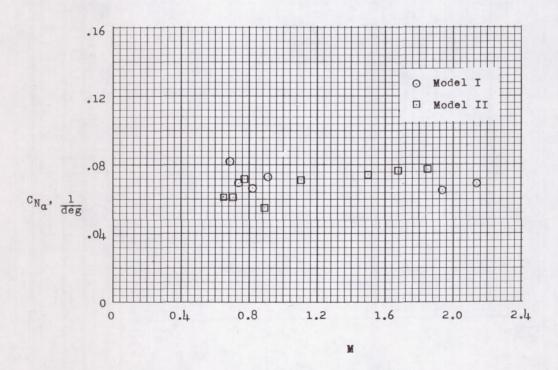Figure 12.- Variation of aerodynamic center with Mach number.

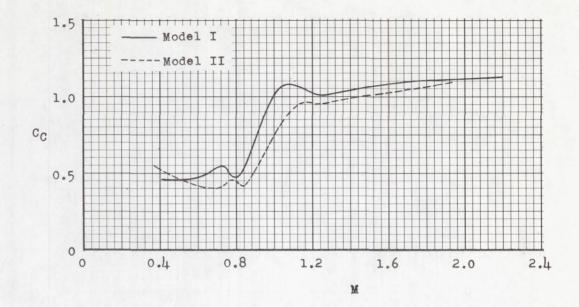Figure 13.- Variation of normal-force-coefficient slope with
Mach number.

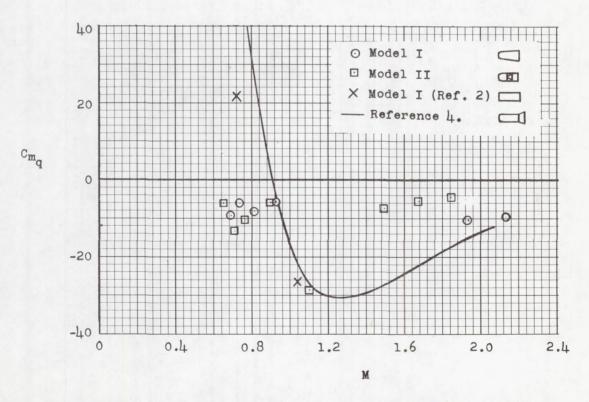Figure 14.- Variation of longitudinal-force coefficient with Mach number.

Figure 15.- Variation of the dynamic stability with Mach number.